Spatial Dependence of Viscosity and Thermal Conductivity through a Planar Interface

ARTICLE *in* THE JOURNAL OF PHYSICAL CHEMISTRY B · FEBRUARY 2009

Impact Factor: 3.3 · DOI: 10.1021/jp807254b · Source: PubMed

2 AUTHORS, INCLUDING:

Janka Petravic
University of New South Wales
77 PUBLICATIONS **733** CITATIONS

SEE PROFILE

THE JOURNAL OF PHYSICAL CHEMISTRY B

Article

Spatial Dependence of Viscosity and Thermal Conductivity through a Planar Interface

Janka Petravic, and Peter Harrowell

J. Phys. Chem. B, **2009**, 113 (7), 2059-2065• Publication Date (Web): 23 January 2009

Spatial Dependence of Viscosity and Thermal Conductivity through a Planar Interface

Janka Petravic* and Peter Harrowell

School of Chemistry, The University of Sydney NSW 2006, Australia

Received: August 14, 2008; Revised Manuscript Received: November 11, 2008

We present a general algorithm for calculating the spatial variation of the shear viscosity and thermal conductivity through an equilibrium solid−liquid interface using the zero-flux version of the boundary fluctuation theory. In the case of an equilibrium interface between a high melting point Lennard-Jones solid and a low melting point Lennard-Jones liquid, we find that the transport coefficients deviate from the bulk values only in a narrow layer close to the interface. We observe a sliding friction of the liquid against the surface of the solid that increases with increased wetting of the solid by the liquid. The thermal conductivity, in contrast, is suppressed in the interfacial region, irrespective of how the liquid wets the solid.

1. Introduction

Transport coefficients in a liquid adjacent to a solid surface vary as a function of the distance from the surface. The conventional approach to treating this variation is to localize the change in transport coefficients to a plane parallel to the interface, converting a spatially varying quantity to a boundary condition of infinitesimal extent. Thus the shear viscosity in the vicinity of the interface is replaced by a slip length, defined as the distance between the interface and the point along the surface normal at which the linear extrapolation of the bulk velocity field vanishes (see Figure 1). The variation of thermal conductivity is replaced by a similarly defined equivalent length. While these boundary conditions are perfectly adequate representations for most hydrodynamic treatments, they omit molecular level detail that is essential to understanding the microscopic origins of interfacial rheology and for the modeling of flow where the fluid extent is of a similar length scale to that over which the transport coefficients vary. To appreciate this loss of information, consider the sketch in Figure 1 of two quite different planar shear flow profiles (related to different spatial variations in the shear viscosity) that give rise to the same slip length.

In this paper we present what we believe to be the first equilibrium calculations of this spatial variation of the shear viscosity and thermal conductivity through the interface between a liquid and a high melting point solid. These calculations provide an explicit definition of local transport coefficients, one formally consistent with the Green−Kubo expressions for the bulk systems. Previously[1] we have shown that equilibrium transport coefficients can be usefully defined across a layer of liquid as small as one molecular diameter. The boundary fluctuation theory,[1−4] described below, makes no distinction between liquid and solid and so treats the response of the solid side of the interface on the same footing as that of the liquid.

Local resolution of viscosity and thermal conductivity, at a suitable coarse-graining scale, is in principle always possible using nonequilibrium simulation methods. These involve either straightforward shearing of planar walls[5−7] or keeping the walls at different temperatures by use of suitable thermostats,[8,9] respectively. A similar class of methods are the heat/momentum exchange methods (HEX or PEX),[10,11] also relying on the constant steady-state fluxes to calculate local transport coefficients from variations of velocity or temperature gradients.

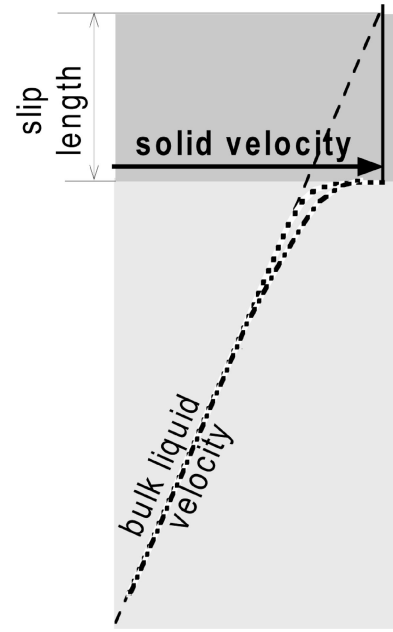

Figure 1. Sketch of construction of the slip length. Two possible velocity fields are shown, both of which give the same slip length. The difference between these fields represents the kind of information that is lost when the spatial variation of transport coefficients is reduced to a slip boundary condition.

The downside of nonequilibrium methods, especially in the case of heat transport, is that different temperatures of two walls change the thermodynamic states of the material between the walls, and therefore the very local transport properties that they aim to measure.[4] In addition, transport coefficients at interfaces involving soft solids such as those found in microemulsions, liquid crystals, and coexisting solid melts cannot be easily studied experimentally or using standard nonequilibrium simulations due to the nonlinear response of these fragile interfaces. The nonlocal equilibrium approach described here avoids this problem. Our goal in this paper is to describe the implementation of the nonlocal version of the boundary fluctuation theory to the study of interfacial transport coefficients.

In the boundary fluctuation theory (BFT),[1−4] we have derived rigorous linear response relations between the transport coefficients and the fluctuations at the explicit boundaries of the

10.1021/jp807254b CCC: $40.75
Published on Web 01/23/2009

sample at which system constraints are applied. The BFT can be formulated either in the zero-gradient ensemble or in the zero-flux ensemble.[2,3] The zero-gradient ensemble for shear viscosity consists of rigorously immobile outer boundaries of the system (container walls); for thermal conductivity the system boundaries are constrained to the same temperature. In this ensemble one can only determine the *average* transport coefficients of the whole heterogeneous material between the walls. We previously applied the zero-gradient BFT to a Lennard-Jones (LJ) solid−liquid system[4] with different degrees of wetting, and estimated the change of viscosity and thermal conductivity of the whole system caused by the presence of the interface. However, their spatial variation in this ensemble could only be seen in nonequilibrium simulations with walls sliding at constant velocity past each other.

In this paper we shall study the zero-flux ensemble, in which the center-of-mass positions and temperatures of the boundary walls are allowed to freely fluctuate. The fluctuations of velocity and temperature differences between the boundary walls determine, respectively, the inverse values of average shear viscosity and thermal conductivity of the material between the walls. In the case of velocity fluctuations we show that the inverse viscosity can be rigorously related to the mutual diffusion of one wall with respect to the other. Because in this ensemble there are no longer constraints on velocities and temperature anywhere within the system, the BFT expressions for transport coefficients can be generalized[1] to find their values in the localized layers of material between arbitrary planes parallel to the system boundaries.

In section 2 we describe our calculations and provide a brief overview of the BFT expressions. In section 3 we present our results in the form of the friction and thermal conductivity coefficients as a function of the normal distance into the liquid from the solid wall. We then compare these local values of the coefficients with the values predicted from previous calculations of the transport coefficients of the entire system (solid and fluid) between the boundary walls. We also examine the rheology of the interfacial region.

2. Simulation Method

Our solid−liquid interface is the result of the equilibrium coexistence of two Lennard-Jones (LJ) species, with the solid species having the significantly higher melting point. The liquid−liquid exclusion diameter σ_L and potential well depth ε_L were set to unity, defining the system of LJ reduced units. In the solid, we chose the exclusion diameter $\sigma_S = 1$ (same as liquid) and the depth of potential well $\varepsilon_S = 10$, which makes the melting temperature of the solid 10-fold higher than that of the liquid. Unlike many models which treat the solid as particles tethered to a crystal lattice, the solid particles in this study are free to fluctuate. Details of this model are provided in ref 4. The liquid−solid pair interaction potential was of the form

$$U_{LS}(r) = 4\varepsilon_{LS}\left[\left(\frac{\sigma_{LS}}{r}\right)^{12} - a_w\left(\frac{\sigma_{LS}}{r}\right)^{6}\right] \qquad (1)$$

with Lorenz−Berthelot rules for the cross-interaction parameters, $\varepsilon_{LS} = (\varepsilon_L\varepsilon_S)^{1/2} = 10^{1/2}$ and $\sigma_{LS} = (\sigma_L + \sigma_S)/2 = 1$, and a variable wetting constant a_w, which determines how closely the liquid atoms are bound to the solid surface. We investigated the interface effects on the system viscosity and thermal conductivity for three values of the wetting constant: $a_w = 1.0$ (liquid atoms are more attracted to the solid than to the other liquid atoms), $a_w = 0.562$ (the solid−liquid interaction is similar to the liquid−liquid interaction), and $a_w = 0.3$ (nonwetting case with liquid atoms bound more strongly to other liquid atoms than to the solid).

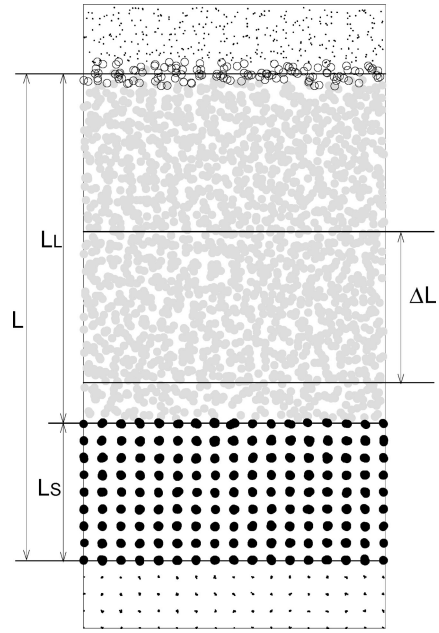

Figure 2. Projection of solid−liquid configurations for $a_w = 0.3$ onto the xz-plane. The frozen boundary atoms are shown as dots, the tethered liquid boundary atoms are shown as open full circles, the freely moving liquid atoms are solid gray circles, and the freely moving solid atoms are solid black circles. The separation of the system boundaries is L, the liquid thickness is L_L and the solid thickness is L_S. The dotted lines show the boundaries of an internal layer of thickness ΔL.

Our system was periodic in the x- and y-directions, with periods $L_x = L_y = 12.4\sigma$. In the z-direction the cell size was $L_z = 28.4\sigma$ for all wetting constants. The cell consisted of coexisting face-centered-cubic (fcc) solid and liquid layers. The reduced temperature of the system was $T = 1.0$, and the reduced pressure was $P = 2.5$. The bulk solid and liquid densities at this state point were $\rho_S = 1.063$ and $\rho_L = 0.841$, respectively. The interface was parallel to the (100) plane of the crystal. The solid layer consisted of 13 crystal planes at average separation of 0.76σ (1536 solid atoms). We created the outer solid boundary by freezing the atoms in the outer four crystal planes, in order to prevent the local changes in crystal plane separations, while providing an environment similar to that in the bulk. The thickness of the remaining "free" solid was $L_S = 6.1$. For the boundary at the upper (liquid) end of the periodic cell, we froze the liquid atoms in the layer of thickness of 2.52σ. Each of the atoms in the layer of thickness 0.7σ below the frozen atoms was tethered to its current site with an anharmonic potential.[4] The amorphous layer of frozen atoms and the tethered layer prevented the escape of liquid atoms out of the cell without disturbing the liquid structure next to the boundary. The thickness of the liquid layer below the outer amorphous boundary was $L_L = 15.6\sigma$. The position of the interface used for the definitions of liquid and solid thickness is arbitrary to a degree (has an ambiguity of $\pm\sigma/2$), which reflects the ambiguity encountered in experiments.[12,13] A representative configuration of the solid−liquid interface for $a_w = 0.3$ (the lowest wetting constant studied) is shown in Figure 2.

In the zero-flux BFT ensemble for viscosity and thermal conductivity, all particles (including at least one boundary) move according to Newton's equations of motion, but the motion of

the rigid boundary frames is constrained in the z-direction. The inverse transport coefficients are obtained from the fluctuations of differences of boundary velocities or temperatures.[1,2] In our system, we chose the rigid solid boundary to be immobile, while the amorphous liquid boundary (the rigid frame and the tethered atoms) was allowed to move freely in the x- and y-directions.

The whole liquid-end boundary (i.e., the frozen atoms in disordered sites and the tethered layer) can be thought of as an infinite flexible molecule with a rigid frame of force centers at the frozen sites, and the tethered layer of atoms attached to it with anharmonic springs. The rigid frame has only two degrees of freedom, whereas all the atoms have three degrees of freedom. In the original derivation[1,2] the Green−Kubo correlation expressions for the inverse transport coefficients were derived for the constant energy ensemble. However, using the constant temperature ensemble, where the temperature of the system is constrained by a homogeneous thermostat, does not change the values of ensemble averages.[14] Therefore, we thermostated all degrees of freedom using a homogeneous Nosé−Hoover thermostat in order to ensure that the system was at the desired state point.

Equations of motion for all free atoms are

$$\dot{\mathbf{r}}_i = \mathbf{p}_i/m$$
$$\dot{\mathbf{p}}_i = \mathbf{F}_i - \alpha\mathbf{p}_i \tag{2}$$

where $\mathbf{r}_i$ and $\mathbf{p}_i$ are position and momentum, respectively, $\mathbf{F}_i$ is the total interaction force on the ith atom, m is its mass (equal to unity for both solid and liquid), and α is the Nosé−Hoover thermostat multiplier. Equations of motion for the tethered atoms j contain, in addition, the anharmonic forces $\mathbf{F}_{\mathrm{anh}}(j)$ arising from the tethering potential described in ref 4.

$$\dot{\mathbf{r}}_j = \mathbf{p}_j/m$$
$$\dot{\mathbf{p}}_j = \mathbf{F}_j + \mathbf{F}_{\mathrm{anh}}(j) - \alpha\mathbf{p}_j \tag{3}$$

The center-of-mass position $\mathbf{r}_{\mathrm{RL}}$ and momentum $\mathbf{p}_{\mathrm{RL}}$ of the rigid frame at the liquid-end boundary are found from

$$\dot{\mathbf{r}}_{\mathrm{RL}} = \mathbf{p}_{\mathrm{RL}}/M_{\mathrm{RL}}$$
$$\dot{\mathbf{p}}_{\mathrm{RL}} = \mathbf{F}_{\mathrm{RL}} - \sum_j \mathbf{F}_{\mathrm{anh}}(j) - \alpha\mathbf{p}_{\mathrm{RL}} \tag{4}$$

In eq 4, $\mathbf{F}_{\mathrm{RL}}$ is the total LJ interaction force acting on the frozen atoms in the liquid boundary, while M_{RL} is the total mass of the rigid liquid frame.

Only the x- and y-components of vectors in eq 4 change in time; the z-components are constant. Although eq 4 contains M_{RL}, the viscosity of the material between the boundaries obtained by our method does not depend on the wall mass. In our simulations, we used the wall mass $M_{\mathrm{RL}} = 80$. The wall-mass independence of BFT results is discussed in the Appendix. The rigid solid boundary atoms were immobile in our simulation.

The Green−Kubo viscosity η of the whole material between the solid-end and liquid-end boundaries can be found from the fluctuations of the velocity of the liquid-end boundary:[1−3]

$$\frac{1}{\eta} = \frac{V}{2k_{\mathrm{B}}T}\int_0^\infty \left\langle \frac{\mathbf{v}_{\mathrm{RL}}(t)}{L}\cdot\frac{\mathbf{v}_{\mathrm{RL}}(0)}{L}\right\rangle \mathrm{d}t \tag{5}$$

where $\mathbf{v}_{\mathrm{RL}}$ is the center-of-mass velocity of the rigid liquid-end frame. $L = 21.7$ is the inner separation between the two ends, i.e., the average separation between the boundary crystal plane and the tethered liquid layer (Figure 1). $V = LS$ is the volume of the material between the walls (S is the cross-section area of the simulation cell parallel to the boundary planes), T is temperature, and k_{B} is the Boltzmann constant. In evaluating eq 5, we used the average of the correlation integrals obtained from x- and y-components of the velocity difference.

Equation 5 directly leads to the equivalent "Einstein" expression for the viscosity of the material between the boundaries in terms of the relative mean square displacement (rmsd) $\langle\Delta\mathbf{r}^2\rangle$ of the boundary planes:

$$\frac{S}{4k_{\mathrm{B}}TL}\langle\Delta\mathbf{r}^2(t)\rangle = \frac{S}{4k_{\mathrm{B}}TL}\langle[\Delta\mathbf{r}_{\mathrm{RL}}(t) - \Delta\mathbf{r}_{\mathrm{RS}}(t)]^2\rangle = \frac{1}{\eta}t \tag{6}$$

where S is the surface area of the simulation cell parallel to the boundaries, and $\Delta\mathbf{r}_{\mathrm{RS}}(t) = \mathbf{r}_{\mathrm{RS}}(t) - \mathbf{r}_{\mathrm{RS}}(0)$ and $\Delta\mathbf{r}_{\mathrm{RL}}(t) = \mathbf{r}_{\mathrm{RL}}(t) - \mathbf{r}_{\mathrm{RL}}(0)$ are the displacements of the solid and the liquid boundaries in time t, respectively. In our simulation, $\Delta\mathbf{r}_{\mathrm{RS}} \equiv 0$. The derivation of the expression eq 6 is presented in the Appendix. The viscosity of the material between the bounding walls is inversely proportional to the mutual diffusion coefficient of the walls, or in our simulation, to the self-diffusion coefficient of one wall when the other is kept immobile.

Thermal conductivity λ of the material between the boundaries is given in terms of fluctuations of temperature difference between the boundary layers[1−3] (in our case the fifth solid plane adjacent to the rigid solid boundary, and the tethered layer):

$$\frac{1}{\lambda} = \frac{V}{k_{\mathrm{B}}T}\int_0^\infty \left\langle \frac{\Delta T(t)}{L}\frac{\Delta T(0)}{L}\right\rangle \mathrm{d}t \tag{7}$$

The Einstein-type relation analogous to eq 6 for the rmsd of relative temperature fluctuations of the boundary walls can also be derived, but it does not have as interesting a physical interpretation as eq 6.

Linear response theory in the zero-flux ensemble also gives access to transport coefficients in layers of material between arbitrary planes of separation ΔL parallel to the boundaries[1,3] (Figure 1). Viscosity $\eta(\Delta L)$, dependent on the position and separation of the inner planes, is determined by the correlations between the strain rate at the boundaries $\Delta v/L$ and the strain rate at the inner planes $\Delta v(\Delta L)/\Delta L$:

$$\frac{1}{\eta(\Delta L)} = \frac{V}{k_{\mathrm{B}}T}\int_0^\infty \left\langle \frac{\Delta\mathbf{v}(\Delta L;t)}{\Delta L}\cdot\frac{\mathbf{v}_{\mathrm{RL}}(0)}{L}\right\rangle \mathrm{d}t \tag{8}$$

Similarly, thermal conductivity $\lambda(\Delta L)$ between the planes separated by ΔL is found from the correlations of the temperature gradient between the boundaries $\Delta T/L$ and temperature gradient between the inner planes $\Delta T(\Delta L)/\Delta L$:

$$\frac{1}{\lambda(\Delta L)} = \frac{V}{k_{\mathrm{B}}T}\int_0^\infty \left\langle \frac{\Delta T(\Delta L;t)}{\Delta L}\frac{\Delta T(0)}{L}\right\rangle \mathrm{d}t \tag{9}$$

All equations of motion were integrated using the Gear predictor−corrector scheme with a time step of 0.001 (in the liquid reduced units). The length of equilibrium runs was 5×10^7 time steps. The values of force or energy flux differences

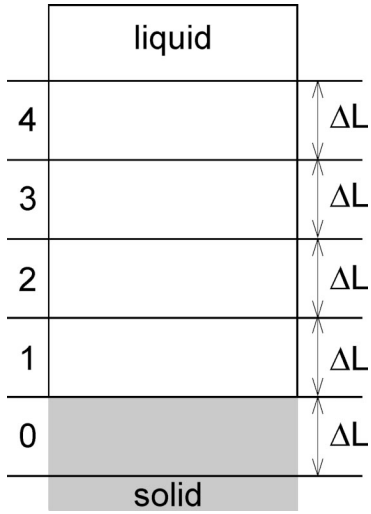

Figure 3. Positions of layers of thickness ΔL in which the local transport coefficients were calculated.

were recorded every five time steps. The correlation functions were calculated using the shifting register technique[15] with a time window of 12 500 records (or 30 000 time steps). Each recorded value was used as an initial point for the averaging of the correlation function.

3. Simulation Results

3.1. Spatial Variation of Equilibrium Transport Coefficients. We measured the local transport coefficients in five layers of equal thickness $\Delta L = 3.36$, shown schematically in Figure 3. Layer 1 was between the last solid crystal plane and the liquid at ΔL distance from it. Layers 2−4 were entirely within the liquid, away from the solid−liquid boundary. Layer 0 was entirely within the solid, with one boundary at the crystal plane next to the liquid.

The values of the transport coefficients in the liquid layers (layers 1−4 in Figure 3) are shown in Figure 4a and Figure 4b for viscosity and thermal conductivity, respectively. Each point represents the coefficient averaged across the layer (the average of the coefficient is the inverse of the average inverse coefficient[4]). The interface is located at $z = 0$. The horizontal line is the value of the coefficient in the bulk liquid ($\eta_L = 2.6$ in Figure 4a and $\lambda_L = 7.2$ in Figure 4b). The transport coefficients deviate from the bulk value only in the liquid layer adjacent to the interface, i.e., a layer 3.36 particle diameters thick. Viscosity is lower than in the bulk liquid for the smallest wetting constant of 0.3, and is higher than the bulk value for the two larger wetting constants. Thermal conductivity is always lower in the interface region than in the bulk and decreases with the decrease in wetting.

3.2. Consistency of Local Transport Coefficients. In Table 1 we have recorded the layer values of the shear viscosity and thermal conductivity calculated from two sets of nonequilibrium molecular dynamics (NEMD) calculations,[4] with constant relative wall velocity $v_{wall} = 0.078$ and constant temperature difference between the walls $\Delta T_{wall} = 0.02$, respectively. In shear flow simulations, the imposed difference in wall velocities gave rise to constant shear stress throughout the liquid and across the solid−liquid interface, different for different wetting constants. Similarly, in heat flow simulations, the heat flux was constant throughout each system, but depended on the interface wetting. Shear stress was evaluated as the average force on the wall opposing its motion, divided by the interface area F_{wall}/S.

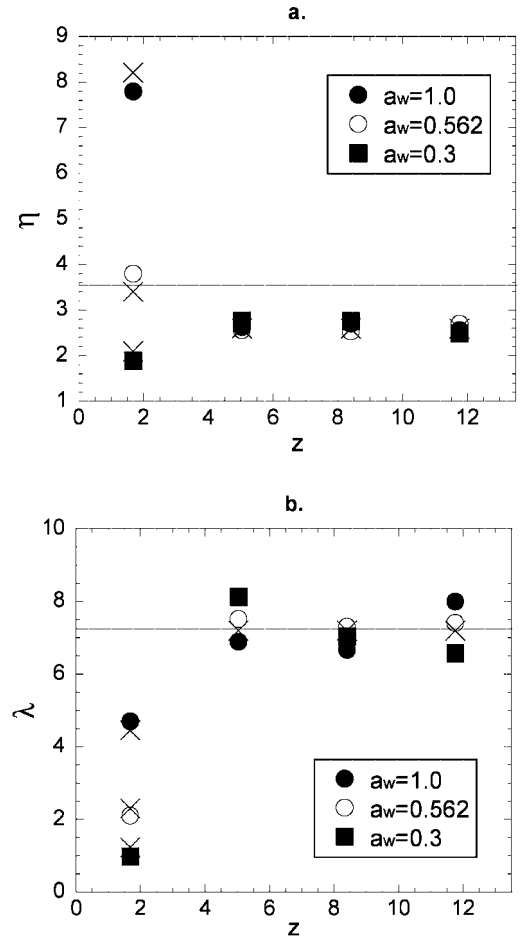

Figure 4. (a) Viscosity and (b) thermal conductivity in liquid layers parallel to the interface. The interface is at $z = 0$. The horizontal line in (a) is the bulk liquid viscosity and in (b) is the bulk liquid thermal conductivity. The crosses are the values of transport coefficients evaluated in the liquid layer next to the boundary using (a) slip length and (b) equivalent liquid length from ref 4.

TABLE 1: Comparison of Local Transport Coefficients Calculated from the Equilibrium BFT and from Simulations of Nonequilibrium Steady States

layer	a_w	η (equilib)	λ (equilib)	η (nonequilib)	λ (nonequilib)
1	0.3	1.9	0.95	2.1	1.2
	0.562	3.7	2.1	3.4	2.3
	1.0	7.8	4.7	8.2	4.5
2	0.3	2.8	8.0	2.6	7.2
	0.562	2.6	7.5	2.7	7.3
	1.0	2.6	6.9	2.6	7.2
3	0.3	2.8	7.0	2.6	7.2
	0.562	2.5	7.3	2.7	7.3
	1.0	2.7	6.8	2.6	7.2
4	0.3	2.5	6.8	2.6	7.2
	0.562	2.7	7.4	2.7	7.3
	1.0	2.6	8.0	2.6	7.2

The heat flux J_Q was found from the Nosé−Hoover thermostat multipliers applied to the walls.[2,4] The transport coefficients in layers 1−4 were determined from the velocity/temperature profiles and the corresponding shear stress/heat flux:

$$\frac{1}{\eta(z)} = \frac{1}{\Delta L}\frac{\Delta v_x(z)}{F_{wall}/S} \tag{10}$$

$$\frac{1}{\lambda(z)} = \frac{1}{\Delta L}\frac{\Delta T(z)}{J_Q} \tag{11}$$

where $\Delta v_x(z) = v_x(z + \Delta L/2) - v_x(z - \Delta L/2)$ is the flow velocity difference between planes separating the layers and similarly for $\Delta T(z)$. We find good agreement between the values of the local transport coefficients calculated via the equilibrium and nonequilibrium methods, indicating that for the interfaces studied the gradients applied in the NEMD calculations were low enough to reach the local linear response in each layer.

It should be noted that, if transport coefficients change with position, the values of local transport coefficients in layers of thickness ΔL would depend on the chosen level of coarse graining, as they would contain spatial averaging over the layer. More precisely, the inverse of the coefficient in a layer would be the average of the inverse coefficient over the layer thickness.

We calculated the values of η and λ in the liquid interface layer predicted by slip lengths obtained from the zero-gradient BFT in the previous paper,[4] assuming that this is the only layer where the changes occur. They are shown as crosses in Figure 4 and are in good agreement with the values obtained in this simulation.

Previous work on viscosity and thermal conductivity at interfaces concentrated on the slip length and the thermal boundary conductance. Our simulation result for the local viscosity of 1.9 in the layer adjacent to the nonwetting interface ($a_w = 0.3$) translates into a slip length of 1.2 molecular diameters. For the wetting surface ($a_w = 1.0$), we observe an adsorbed layer of 2 molecular diameters. This agrees with the other reported simulation results with similar parameters.[5−7] Our result would correspond to a slip length of 4.2 Å for liquid argon at the temperature 120 K and a pressure of 100 MPa next to a nonwetting solid interface, which is orders of magnitude less than the slip length of 19 nm measured for ambient water next to a hydrophobic surface.[13] Possible reasons for such a small slip in simulation results are the choice of the same sizes for solid and liquid atoms, and relatively high pressure. The fact that we used an unconstrained solid−liquid interface, instead of a frozen or harmonically tethered solid, may have also contributed to increased momentum transfer between liquid and solid.

The equivalent liquid lengths estimated from the thermal conductivity of the layer of liquid next to the interface are 17 molecular diameters for the nonwetting case and 2.1 for the wetting case. These results are similar to the values of 12 and 5 found in a nearly identical LJ system near the triple point.[8] Barrat and Chiarrutini[9] got approximately 3 times larger equivalent lengths for a similar choice of parameters but at a very low pressure. Translated into values for liquid argon, our results would correspond to a thermal boundary conductance of 660 MW m^{-2} K^{-1} at a wetting interface and 82 MW m^{-2} K^{-1} at a nonwetting interface. These results are the same order of magnitude as the conductances measured at hydrophilic (180 MW m^{-2} K^{-1}) and hydrophobic (60 MW m^{-2} K^{-1}) Al−water interfaces.[16]

The correlation integrals eq 8 for viscosity and eq 9 for thermal conductivity (as a function of the upper time limit) in the liquid layer next to the interface for three wetting constants are shown in Figure 5a and Figure 5b, respectively. These integrals provide a sense of how the time integral of the fluctuation correlator converges to the final value of the transport coefficient. The viscosity correlation integrals show oscillations caused by transverse waves in the solid plane adjacent to the liquid, which is one of the boundaries of the interface liquid layer. There is also a small delay in the propagation of the strain rate across the interface, similar to the delay observed in constant-flux BFT simulations of pure liquid.[1] The amplitude of the oscillations decreases with the decrease in wetting, while the delay increases. The oscillations and the delay are too small to be observed in correlations of the temperature gradient across the interface (Figure 5b).

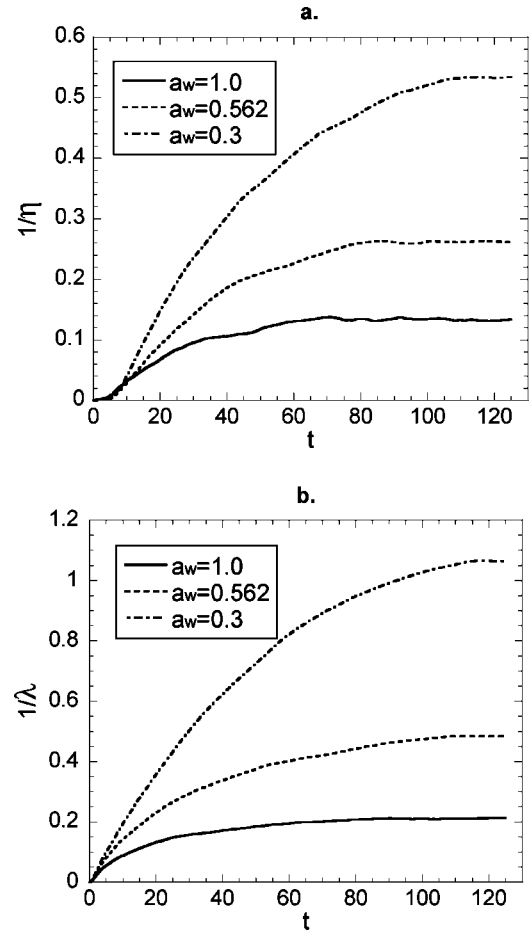

Figure 5. Correlation integrals as functions of the upper time limit for (a) viscosity using eq 7 and (b) thermal conductivity using eq 8 in the liquid layer next to the solid surface for three wetting constants.

4. Conclusion

We have calculated spatially dependent linear response viscosity and thermal conductivity in layers of thickness of several atomic diameters parallel to a solid−liquid interface using boundary fluctuation theory in the zero-flux ensemble. In the liquid phase, the transport coefficients deviate from the bulk values only in the layer closest to the interface. In the system with the weakest wetting, viscosity is lower than in the bulk liquid, while for the two systems with stronger wetting the viscosity is higher because of liquid atoms adsorbed on the solid surface. Thermal conductivity in the liquid layer next to the solid surface is always below the bulk thermal conductivity, but it increases with the degree of wetting. In the solid layer next to the interface, viscosity is very large but finite and decreases with the decrease in solid−liquid interactions. The results are in good agreement with the results obtained in the zero-gradient ensemble[4] in systems of smaller size but with the same interface characteristics.

The derivation of a rigorous expression relating the viscosity of the confined media and the mutual diffusion (relative mean

square displacement) of the confining surfaces in the zero flux ensemble, presented in eq 6, is noteworthy. The expression is of the same origin (the double time integral of the Green−Kubo correlation function) as the "Einstein expressions" for viscosity and thermal conductivity in periodic boundary conditions,[17] and the momentum correlation function for the friction coefficient of two Brownian particles.[18] However, only in the case of zero-flux BFT has the displacement function such a simple physical meaning, directly linking viscosity to another transport coefficient. The result expressed in eq 6 says that if the material between the boundaries has a finite viscosity, then the boundaries will diffuse with respect to each other. Conversely, one can calculate the viscosity of the material between the boundaries from the external forces that one has to apply on the boundaries to prevent them from diffusing with respect to each other. This is what is done in the zero shear rate ensemble.

Acknowledgment. The authors would like to acknowledge the support of the Australian Research Council through the Discovery program. A generous grant of computer time from the Australian Partnership for Advanced Computing is gratefully appreciated.

APPENDIX: Viscosity Correlation Integrals Are Independent of Wall Masses

The expression for viscosity, eq 5, relates the viscosity of the material between the outer boundaries to the correlations of fluctuations in the relative center-of-mass velocities of the outer boundaries of the system. In our simulation, the outer boundaries consist of frozen external layers and tethered atoms. The frozen external layers play the role of an external force field that keeps the boundary layers at constant separation and the phases within at a desired structure. However, the nature of fluctuations in the center-of-mass velocities of these boundary walls strongly depends on the mass of the walls, which can, in principle, be assigned any value. On the other hand, the viscosity of the material between the boundaries should depend only on interactions and should not be affected by the wall mass.

Using the Langevin equations for the wall motion, we show here that the plateau value of eq 5 and the slope of the relative mean square displacement in the long-time limit, eq 6, are independent of wall masses.

The Langevin equations for the motion of the two walls are

$$M_1\dot{v}_1 = F_D + A_1(t)$$
$$M_2\dot{v}_2 = -F_D + A_2(t) \tag{A1}$$

where M_1 and M_2 are the masses of wall 1 and wall 2, and A_1 and A_2 are the stochastic forces acting on them. The hydrodynamic drag forces $\pm F_D$ acting on the walls are of equal magnitude and opposite direction, and are caused by shear stress when sliding one wall with respect to the other. If the wall surface area is S, the wall separation is L, and v_1 and v_2 are wall velocities, then the shear stress in the system is F_D/S, and the strain rate is $(v_1 - v_2)/L$, so that the drag force on wall 1 satisfies the relationship

$$\frac{F_D}{S} = -\eta\frac{v_1 - v_2}{L} \tag{A2}$$

where η is the viscosity of the material between the walls. Substituting eq A2 into the system eq A1 and after some manipulation, we obtain a standard Langevin equation for the wall velocity difference $\Delta v = v_1 - v_2$:

$$\frac{d}{dt}\Delta v = -\zeta\Delta v + A(t) \tag{A3}$$

with the friction coefficient

$$\zeta = \eta\frac{S}{L}\left(\frac{1}{M_1} + \frac{1}{M_2}\right) \tag{A4}$$

and the δ-correlated stochastic force

$$A(t) = \frac{A_1(t)}{M_1} + \frac{A_2(t)}{M_2} \tag{A5}$$

satisfying the fluctuation−dissipation relationship

$$\int_{-\varepsilon}^{+\varepsilon}\langle A(0)\,A(t)\rangle\,dt = 4\zeta k_B T\left(\frac{1}{M_1} + \frac{1}{M_2}\right) \tag{A6}$$

where ε is an arbitrarily short time interval. There is a factor of 4 because there are only two degrees of freedom for the thermal motion of the wall in our model.

The solution of eq A3 for the average relative mean square displacement (rmsd) of the walls is given by[19]

$$\langle\Delta r^2\rangle = \frac{\Delta v_0^{\,2}}{\zeta^2}(1 - e^{-\zeta t})^2 + \frac{2k_B T}{\zeta^2}\left(\frac{1}{M_1} + \frac{1}{M_2}\right)(2\zeta t - 3 + 4e^{-\zeta t} - e^{-2\zeta t}) \tag{A7}$$

for the walls having the initial relative wall velocity at $t = 0$ equal to Δv_0. In the short time limit (retaining only terms up to second order in t in eq A7) the average rmsd depends on the initial relative velocity and is proportional to t^2:

$$\langle\Delta r^2\rangle = \Delta v_0^{\,2} t^2 \tag{A8}$$

The rmsd averaged over all equipartition-distributed initial relative velocities would then be

$$\langle\Delta r^2\rangle = 2k_B T\left(\frac{1}{M_1} + \frac{1}{M_2}\right)t^2 \tag{A9}$$

That is, it is smaller when the walls have larger masses. However, in the long-time limit

$$\langle\Delta r^2\rangle = \frac{4k_B T}{\zeta}\left(\frac{1}{M_1} + \frac{1}{M_2}\right)t = \frac{4k_B TL}{\eta S}t \tag{A10}$$

rmsd is proportional to t and with the relative diffusion coefficient $D = k_B TL/(\eta S)$ is independent of mass.

According to eqs 5 and A10, the inverse viscosity is equal to

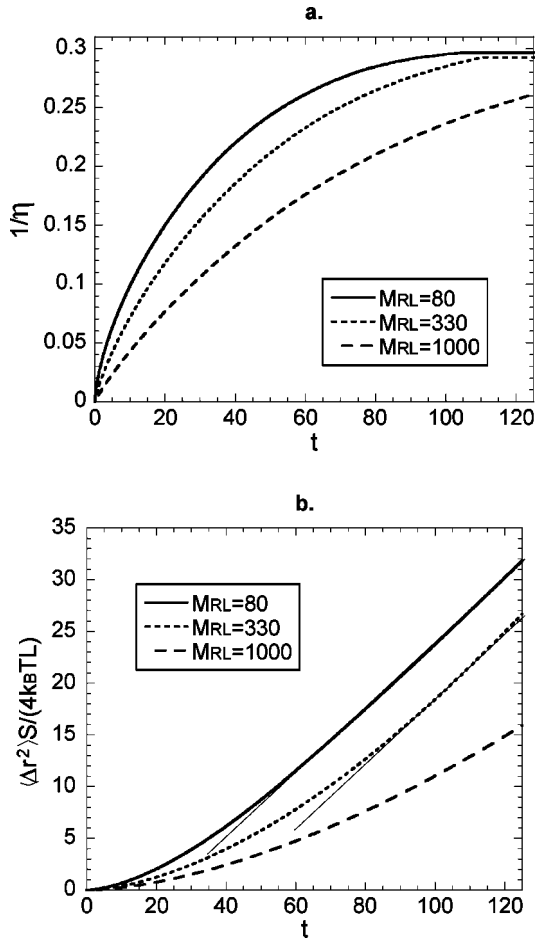

Figure 6. (a) Dependence of viscosity correlation integral, eq 7, on rigid wall mass for the system with $a_w = 0.3$. (b) Time dependence of mean square displacement of the walls.

$$\frac{1}{\eta} = \frac{S}{2k_B TL}\int_0^\infty \langle \mathbf{v}(t)\cdot\mathbf{v}(0)\rangle \, dt = \frac{S}{k_B TL}D \qquad \text{(A11)}$$

i.e., proportional to the long-time limit of the diffusion coefficient and independent of wall mass. However, if the wall mass is larger, the correlation time needed for the correlation integral to reach the plateau gets longer. The results for the immobile solid boundary (as used in our simulation) correspond to one of the wall masses being infinite, and the other being equal to M_{RL}.

In order to illustrate this point, we have simulated the same solid−liquid system with the wetting constant $a_w = 0.3$ with the mass of the rigid liquid-end wall frame equal to $M_{RL} = 80$, 330, and 1000. The results for the correlation integrals eq 5 and the rmsd eq 6 are shown in Figure 6a and Figure 6b, respectively. The correlation time increases with the increase in wall mass, while the long-time limit is independent of mass. The correlation integral in Figure 6a for $M_{RL} = 1000$ has not reached the plateau value within the time window. In Figure 6b, the slopes for the two smaller masses in the long-time limit are the same, while within the time window used the wall with the largest mass has not reached the linear dependence of rmsd.

Although the plateau value of the correlation integral eq 5 is independent of wall mass, the simulation becomes more efficient if it is chosen to be as small as practically possible (in order not to necessitate the use of smaller time steps in the integrator). If the mass is smaller, it is possible to use shorter time windows and get better statistics in simulations of the same lengths.

References and Notes

(1) Petravic, J.; Harrowell, P. *J. Chem. Phys.* **2006**, *124*, 044512.
(2) Petravic, J.; Harrowell, P. *Phys. Rev. E* **2005**, *71*, 061201.
(3) Petravic, J.; Harrowell, P. *J. Chem. Phys.* **2006**, *124*, 014103.
(4) Petravic, J.; Harrowell, P. *J. Chem. Phys.* **2008**, *128*, 194710.
(5) Thompson, P. A.; Robbins, M. O. *Phys. Rev. A* **1990**, *41*, 6830.
(6) Barrat, J.-L.; Bocquet, L. *Phys. Rev. E* **1994**, *49*, 3079.
(7) Thompson, P. A.; Troian, S. *Nature* **1997**, *389*, 360.
(8) Xue, L.; Keblinski, P.; Phillpot, S. R.; Choi, U.-S.; Eastman, J. A. *J. Chem. Phys.* **2003**, *118*, 337.
(9) Barrat, J.-L.; Chiarrutini, F. *Mol. Phys.* **2003**, *101*, 1605.
(10) Guo, H.; Kremer, K.; Soddemann, T. *Phys. Rev. E* **2002**, *66*, 061503.
(11) Simon, J.-M.; Kjelstrup, S.; Bedeaux, D.; Hafskjold, B. *J. Phys. Chem. B* **2004**, *108*, 7186.
(12) Vinogradova, O. I. *Langmuir* **1995**, *11*, 2213.
(13) Cottin-Bizonne, C.; Cross, B.; Steinberger, A.; Charlaix, E. *Phys. Rev. Lett.* **2005**, *94*, 056102.
(14) Evans, D. J.; Sarman, S. *Phys. Rev. E* **1993**, *48*, 65.
(15) Allen, M. P.; Tildesley, D. J. *Computer Simulation of Liquids*; Clarendon: Oxford, 1987.
(16) Ge, Z.; Cahill, D. G.; Braun, P. V. *Phys. Rev. Lett.* **2006**, *96*, 186101.
(17) Helfand, E. *Phys. Rev.* **1960**, *119*, 1.
(18) Bocquet, L.; Hansen, J.-P.; Piasecki, J. *J. Stat. Phys.* **1997**, *89*, 321.
(19) McQuarrie, D. A. *Statistical Mechanics*; University Science Books: New York, 2000.

JP807254B